

Surface Functionalization of Supported Mn Clusters to Produce Robust Mn Catalysts for Selective Epoxidation

Satoshi Muratsugu,^{*,†,‡} Zhihuan Weng,^{†,||} and Mizuki Tada^{*,†,‡,§}

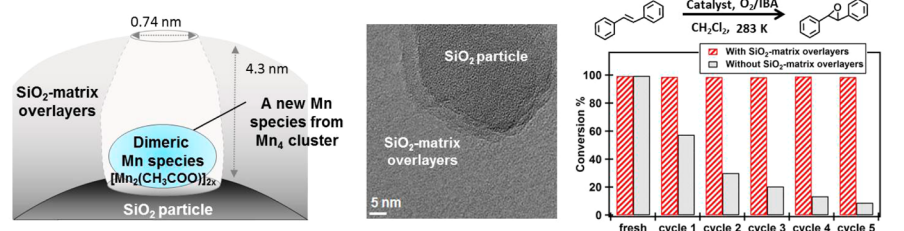
[†]Institute for Molecular Science, 38 Nishigo-naka, Myodaiji, Okazaki, Aichi 444-8585, Japan

[‡]Department of Chemistry, Graduate School of Science, and [§]Research Center for Materials Science, Nagoya University, Furo-cho, Chikusa, Nagoya 464-8602, Japan

^{||}Department of Applied Physics and Chemistry, The University of Electro-Communication, Chofu, Tokyo 182-8585, Japan

Supporting Information

Robust heterogeneous catalysis on functionalized surface with a new Mn species



ABSTRACT: A robust heterogeneous Mn catalyst for selective epoxidation was prepared by the attachment of a Mn₄ oxonuclear complex [Mn₄O₂(CH₃COO)₇(bipy)₂](ClO₄)·3H₂O (1) on SiO₂ and the successive stacking of SiO₂-matrix overlayers around a supported Mn cluster. The structures of supported Mn catalysts were characterized by means of FT-IR spectroscopy, diffuse-reflectance UV/vis spectroscopy, Raman spectroscopy, X-ray photoelectron spectroscopy, and Mn K-edge X-ray absorption fine structure. A ligand exchange reaction between the CH₃COO ligand of 1 and surface silanol group produced a SiO₂-supported Mn cluster (2), whose coordination structure was similar to 1. Subsequent heating of 2 under vacuum yielded supported Mn clusters (3, 4) through the partial elimination of CH₃COO ligands. The surface-attached Mn clusters of 2, 3, and 4 were easily released to a reaction solution under epoxidation conditions (Mn leaching: approximately 50%), although they were active for epoxidation of *trans*-stilbene (the conversion of *trans*-stilbene, 99%, and the selectivity of *trans*-stilbene epoxid, 96%, for 6 h on 3). We found that the functionalization of the supported Mn cluster on 2 with surface SiO₂-matrix overlayers altered the reactivity of the supported Mn cluster. Dimeric Mn species (5c) with reduced Mn oxidation state and coordination numbers was formed together with a reaction nanospace surrounded by the SiO₂-matrix overlayers. By optimizing the stacking manner of the SiO₂-matrix overlayers, the durability of the Mn catalyst was remarkably improved from leaching (the Mn leaching reached the minimum value of 0.01%), and active and stable epoxidation performances were successfully achieved in the heterogeneous phase (the conversion of *trans*-stilbene, 97%, and the selectivity of *trans*-stilbene epoxide, 91%, for 31 h on 5c).

KEYWORDS: Mn cluster, SiO₂ particles, surface functionalization, SiO₂-matrix overlayers, selective epoxidation

1. INTRODUCTION

Creating a new catalytically active and stable species from transition metal complexes and clusters remains a fundamental challenge in catalysis. The catalytic properties of homogeneous transition metal complexes can be fine-tuned by using various combinations of metal ions and ligands at a molecular level.¹ However, coordination structures are likely to decompose during the homogeneous catalytic reaction conditions and tend to lose catalytic activity, for instance, through aggregation of metal complexes forming inactive species.

The heterogenization of homogeneous metal complexes and clusters by grafting or anchoring to a solid surface, or by immobilizing in polymers or porous materials, has been widely adopted to produce more stable metal complexes during catalytic reaction as well as to produce unique catalytically

active metal species.^{2,3} The site isolation effect on solid surfaces prevents metal complexes and clusters from undergoing aggregation that will result in deactivation, and makes them easier to separate from reaction media for recycling.^{2,3} However, the chemical grafting of a metal complex on a support does not always give a stable catalytically active metal species, and leaching of the metal species from the surface often proceeds under catalytic reaction conditions. This phenomenon occurs when chemical bonding between a metal complex and an oxide surface is relatively weak and does not last sufficiently long under the catalytic conditions.

Received: January 25, 2013

Revised: July 18, 2013

One notable example is a catalyst system using 3d-metal complexes (Mn and Fe) under oxidation reaction conditions. Mn complexes and clusters,⁴ such as Mn porphyrines,⁵ Mn salens,⁶ and Mn 1,4,7-triaza-1,4,7-trimethylcyclononane (tmtacn) complexes,⁷ were reported to be promising oxidation catalyst precursors because their derivatives exhibit high activity and selectivity for oxidation of alkenes and alcohols. In some cases, they could be used with mild oxidants such as O₂ and H₂O₂. Mn oxonuclear clusters with acetate and phosphate ligands have attracted considerable attention because they were potential models of metal enzyme active sites,^{4b,8} such as catalase⁹ and the water oxidation center in Photosystem II.¹⁰ The activity for oxidation of alcohols,¹¹ epoxidation and *cis*-dihydroxylation of alkenes,^{7h-j,11b,12} sulfoxidation,^{11b,13} and oxidation of alkanes^{11b,14} were reported. In spite of these intriguing properties, Mn complexes and clusters tend to decompose and lose their catalytic activities in homogeneous conditions.

The heterogenization of Mn complex catalysts has also been investigated with the aim to increase catalytic activity and catalyst stability. Grafting of Mn porphyrine and salen complexes inside mesoporous materials was among the first methods used to prepare heterogeneous Mn complex catalysts. Various supports were used for this purpose, including zeolites,¹⁵ mesoporous SiO₂,¹⁶ clays,¹⁷ zinc–aluminum double hydroxides,¹⁸ and carbon.¹⁹ However, Mn species sometimes leached into the solution phase. Covalent anchoring of Mn salen complexes on oxide surfaces or inside mesoporous materials via organic linkers was reported to be effective for dramatically enhancing their stability and recyclability in oxidation reactions without changing the structure of Mn complexes.²⁰ Coordination of Mn ions to surface-functionalized ligands yielded site-isolated supported Mn complex catalysts that were highly stable for epoxidation reactions.²¹ Grafting of a Mn(tmtacn) dinuclear cluster on a carboxylate-functionalized oxide surface enabled in situ production of a catalytically active Mn dinuclear cluster with a degree of stability.²² Other efficient reported approaches for heterogenization were the incorporation of Mn complexes inside polymers, ionic liquids, and metal–organic frameworks.^{23–25} The grafted- or supported Mn complexes introduced here had basically similar structures to precursor complexes; therefore, the generation of totally new catalytically active Mn species from the original Mn complexes was quite rare.

Here we report a new catalytically active Mn species through functionalization of a Mn cluster-attached SiO₂ surface toward robust epoxidation catalysis in a heterogeneous phase. A Mn oxotetranuclear cluster, [Mn₄O₂(CH₃COO)₇(bipy)₂](ClO₄)·3H₂O (**1**),^{26a} which has been prepared as a series of model complexes for Photosystem II,^{26,27} was chemically attached on the surface of SiO₂ particles by reaction with surface Si–OH groups. However, the chemical bond attaching the complex at the interface was found to be easily cleaved under epoxidation reaction conditions. We functionalized the Mn cluster-attached SiO₂ surface by stacking SiO₂-matrix overlayers through the method we have developed, and the space around the supported Mn cluster was filled by the matrix overlayers. This surface functionalization remarkably changed the epoxidation performances of the Mn catalyst on the SiO₂ surface, and the robust epoxidation performances were achieved on the Mn catalyst in a heterogeneous phase.

2. EXPERIMENTAL SECTION

2-1. Preparation of [Mn₄O₂(CH₃COO)₇(bipy)₂](ClO₄)·3H₂O (1**).** All reagents were purchased from Sigma-Aldrich, STREM, Wako Chemicals, and Tokyo Kasei Kogyo, and used as received unless otherwise noted. [Mn₃O(CH₃COO)₆(py)₃](ClO₄) was prepared by the literature method²⁸ and [Mn₄O₂(CH₃COO)₇(bipy)₂](ClO₄)·3H₂O (**1**) was synthesized by literature reported procedure with modifications.^{26a}

Under N₂ atmosphere, 2,2'-bipyridine (bipy) (1.15 g, 7.36 mmol) was added to a stirred MeCN solution (50 mL) of [Mn₃O(CH₃COO)₆(py)₃](ClO₄) (2.06 g, 2.36 mmol). The solution was stirred at room temperature for 1 h, and the resulting deep red solution was mixed with a 1:1 mixture of hexane and Et₂O (50 mL) and additional Et₂O (20 mL). The powder was collected by filtration, washed with Et₂O, and dried; yield 70.9% (from Mn basis). Compound **1** was obtained as a dark red powder in trihydrate form. Anal. Calcd for C₃₄H₄₃N₄O₂₃ClMn₄: C, 36.11; H, 3.83; N, 4.95%. Found: C, 36.29; H, 3.65; N, 5.14. ¹H NMR (CD₂Cl₂): −130.5, −77.0, −29.7, −19.3, −18.8, −11.5, 20.2, 22.8, 28.0, 33.2, 36.4, 45.2. ESI-TOF MS (CH₂Cl₂): *m/z* 976.9320 [M]⁺ (Calcd for C₃₄H₃₇O₁₆N₄Mn₄, 976.9727) (Supporting Information, Figure S1).

2-2. Preparation of SiO₂-Supported Mn₄ Cluster (2**).** SiO₂ (1 g, Aerosil 200, Degussa, surface area: 200 m² g^{−1}) was calcined at 673 K for 2 h and kept under vacuum for 0.5 h prior to the grafting of **1**. The precalcined SiO₂ (1 g) was suspended in CH₂Cl₂ (20 mL) under N₂, and a CH₂Cl₂ solution (10 mL) of **1** (0.114 g, 1.01 × 10^{−4} mol) was added. After stirring for 0.5 h, the solvent was removed under reduced pressure, and the resulting solid was allowed to dry under vacuum for another 1–2 h. Loading of Mn was evaluated by X-ray fluorescence (XRF) to be 2.2 wt %, which corresponded to the surface density of **1** to be 0.3 nm^{−2} (approximately one-third of the maximum surface density). Catalyst **2** with low Mn loading (surface density of **1**: 0.2 and 0.1 nm^{−2}) was prepared in a similar way. Catalysts heated for 3 h at 373 and 413 K under vacuum were also prepared (**3** and **4**).

2-3. Stacking of SiO₂-Matrix Overlayers. A SiO₂ matrix protecting Mn catalyst (**5a**) was prepared as follows. Tetramethoxysilane (TMOS, Si(OCH₃)₄) (0.67 g (0.65 mL)) and distilled H₂O (0.27 mL) were placed in glass reactors connected to a two-necked flask containing a supported Mn cluster (**2**, 0.2 g). After the whole system was evacuated to prepare a closed system with reduced pressure, the glass reactors were heated to 393 K and chemical vapor deposition (CVD) was used to vaporize TMOS and H₂O and deposit them on a supported Mn cluster catalyst. During the CVD process, the catalyst was vigorously stirred at room temperature. Then, the two-necked flask was separated from the glass reactor while maintaining the closed system, and hydrolysis–polymerization of TMOS was performed at 358 K for 24 h. The whole closed system was subsequently evacuated at 373 K for 4 h. A Mn catalyst protected by a SiO₂ matrix (**5b**) was prepared in a similar way with double the amounts of TMOS (1.34 g) and H₂O (0.54 mL). A Mn catalyst protected by a SiO₂ matrix (**5c**) was prepared by twice performing the procedure of stacking SiO₂-matrix overlayers of TMOS (0.67 g) and H₂O (0.27 mL). Weight gain after the hydrolysis–polymerization was measured after evacuation at 373 K, and the ratio of polycondensed TMOS was estimated.

2-4. Preparation of SiO₂-Supported MnO_x Catalysts. **2** was heated for 3 h at 673 K under vacuum to prepare catalyst **6**. Catalyst **7** was prepared by the stacking of SiO₂-matrix overlayers on **6** similar to the preparation of **5c**.

2-5. Catalyst Characterization. XRF was measured on a JEOL JSX-3400RII spectrometer. The loading of Mn on the solid samples was determined by using standard curves of Mn K α and Si K α . The amount of CH₃COO ligands released from Mn clusters during the attachment to SiO₂ was determined as follows. After the impregnation of SiO₂ with **1** in a Schlenk tube under N₂ atmosphere, the resulting supernatant was decanted from the suspension, and the released CH₃COOH was dissolved and quantified by gas chromatography using a flame ionization detector (FID-GC; Shimadzu GC-14B, CHIRALDEX B-DM column). The number of CH₃COO ligands in **2**, **3**, **4**, and **5c** were determined as follows. The catalysts were treated with excess amount of CF₃COOH in CH₂Cl₂ solution, and the removed CH₃COOH was quantified by FID-GC (Shimadzu GC-14B, CHIRALDEX B-DM column).

FT-IR spectra were recorded in transmission mode with 4 cm⁻¹ resolution on a JEOL JIR-7000 spectrometer. A KBr disk of Mn₄ cluster (**1**) was evacuated under vacuum for 1 h in an in situ IR cell equipped with NaCl windows before FT-IR measurements. FT-IR spectra of **2**, **3**, and **4** were measured under in situ conditions using a neat disk of **2** prepared under N₂ atmosphere. The sample was evacuated for 1 h, and the spectrum of **2** was recorded. Then the sample was heated under vacuum for 1 h at 373 K and that of **3** was recorded. Finally, it was heated under vacuum for 1 h at 413 K and that of **4** was recorded.

Transmittance and diffuse-reflectance (DR) UV/vis spectra were recorded on a JASCO V-550-DS spectrometer equipped with an integrating sphere. **1** was dissolved in CH₂Cl₂. Solid **2**, **3**, **4**, and **5** were placed in quartz cells under Ar atmosphere.

²⁹Si solid-state magic angle spinning (MAS) NMR spectra were recorded with a JEOL JNM-ECX400 spectrometer operating at 79.5 MHz. A single-pulse detection method was used in ²⁹Si NMR measurements, and a sample was set in a zirconia rotor of 4 mm in diameter and rotated at 10 kHz with a relaxation delay time of 3 s. Sodium 3-(trimethylsilyl)propionate-2,2,3,3-*d*₄ (²⁹Si: 0 ppm) was used as an external standard for the calibration of chemical shifts. Accumulation numbers were fixed at about 10,000.

X-ray photoelectron spectroscopy (XPS) was measured on a VG ESCALAB 220i-XL apparatus at a base pressure of 1 × 10⁻⁷ Pa. The X-ray source, voltage, and current were Mg-K α , 15 kV, and 20 mA, respectively. Binding energies were referenced to those of C 1s (284.8 eV) for **1** and Si 2p (103.4 eV) for **2-5**.

Nitrogen adsorption was measured on a Micromeritics ASAP-2020 analyzer (Shimadzu) at 77 K. Each sample (100 mg) was degassed at 373 K for 2 h under vacuum before an adsorption measurement, and the dead volume was estimated by using He.

X-ray absorption fine structure (XAFS) spectra at the Mn K-edge were measured at the BL-9C and BL-12C stations of the Photon Factory at KEK-IMSS. The energy and current of the electrons in the storage ring were 2.5 GeV and 450 mA, respectively. X-rays from the storage ring were monochromatized by Si(111) double crystals. Mn K-edge XAFS of **1** and SiO₂-supported Mn catalysts were measured in transmission mode, and ionization chambers filled with pure N₂ gas and a mixture of N₂ and Ar gases (15/85, v/v) were used to monitor the incident and transmitted X-rays, respectively. Mn catalysts

protected by SiO₂-matrix overlayers were measured in fluorescence mode, and an ionization chamber filled with N₂ and a Lytle detector filled with Ar were used to monitor the incident and fluorescence X-rays, respectively. All samples were measured at 20 K under vacuum. Because of low Mn loading on **5c**, Aerosil 300 was also used as a support for the XAFS measurements of **5c**.

Mn K-edge XAFS spectra were analyzed with the ATHENA and ARTEMIS programs using the IFEFFIT suite (ver. 1.2.11).²⁹ Mn K-edge XANES spectra were calibrated with Mn foil to the first inflection point of the edge, an energy of 6539.0 eV.³⁰ For Mn K-edge EXAFS analysis, the threshold energy was tentatively set at the first inflection point of the Mn K edge, and background was subtracted by the Autobk method.^{29a,31} *k*³-Weighted extended EXAFS oscillations were Fourier transformed into *R*-space, and single-scattering curve-fitting analysis was performed in *R*-space with coordination number (CN), interatomic distance (*R*), Debye–Waller factor (σ^2), and correction-of-edge energy (ΔE_0) as fitting parameters. Phase shifts and backscattering amplitudes for Mn···Mn and Mn–O(N) were calculated with the FEFF8 code³² from the coordinates of **1** obtained from X-ray single-crystal structural data.^{26c} For the curve fitting of **1**, CNs and bond distances were fixed as the average values obtained from X-ray single crystal structural analysis.

2-6. Catalytic Epoxidation of Alkenes. Each catalyst (Mn4: 0.67 × 10⁻⁶ mol) was suspended in a CH₂Cl₂ solution (3 mL) under 101.3 kPa of O₂ in a closed glass reactor equipped with a mechanical stirrer. Alkene epoxidation reactions were conducted at 283 K by the addition of an alkene reactant, biphenyl as an internal standard, and isobutyraldehyde (IBA) to the suspension (Mn₄/reactant/biphenyl/IBA = 1/500/250/1500 in molar ratio). To monitor the reaction, reactants and products were analyzed by GC (Shimadzu GC-14B, CHIRALDEX G-TA column) using an internal standard and by GC-MS (Shimadzu GC-2010, CHIRALDEX B-DM column) at appropriate intervals. Inductively coupled plasma (ICP) measurements to estimate Mn amounts in solutions were performed with a plasma spectrometer (SPS 7800, SII Seiko Instrument Inc.). Activation energy (*E*_a) was estimated in the temperature range of 283–303 K. After epoxidation of cholesteryl benzoate, the product ratio of α -epoxide/ β -epoxide was estimated by ¹H NMR.^{33a}

3. RESULTS AND DISCUSSION

3-1. Preparation and Characterization of Supported Mn Clusters on a SiO₂ Surface. Chemical grafting of metal complexes allows for easy separation of catalyst from reagents, and prevents the aggregation of metal complexes that lead to deactivation.^{3,20–22} However, the simple chemical grafting of metal complexes on a support does not always give a stable metal site as catalytically active species, and leaching of the metal species from the surface often proceeds under catalytic reaction conditions.^{15–19} We have proposed the design of molecularly imprinted metal-complex catalysts on SiO₂ surfaces using SiO₂-matrix overlayers for imprinting a ligand of a supported metal complex.³⁴ The hydrolysis–polymerization of TMOS deposited on the surface with attached metal complexes can produce surface SiO₂-matrix overlayers on the SiO₂ surface, whose height can be easily regulated.³⁴ Significant improvements in catalytic performance have been observed on molecularly imprinted metal complex catalysts on SiO₂.³⁴

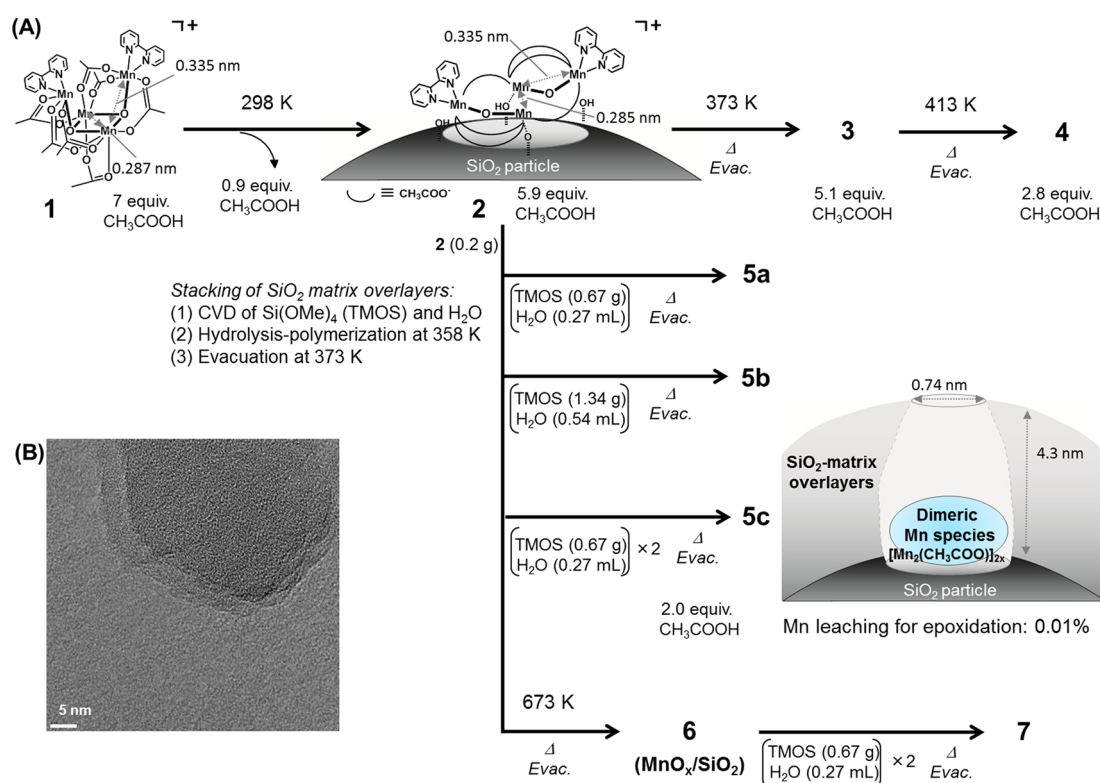


Figure 1. (A) Schematics of the attachment of the Mn_4O_2 cluster (1) on the surface of SiO_2 and surface functionalization with SiO_2 -matrix overlays to produce nanopores protecting the supported Mn cluster. (B) HRTEM images of a SiO_2 particle of 5c with the SiO_2 matrix. The average particle size of Aerosil 200 support was 12 nm (reported by the product company), but it was difficult to visualize SiO_2 overlays on such small particles, which gathered each other.

Motivated by these researches, this technique was employed to try to stabilize a Mn cluster supported on the surface of SiO_2 particles. The SiO_2 -supported Mn cluster catalyst was active for epoxidation but easily leached to reaction solutions. The surface of the SiO_2 particles with the Mn cluster was functionalized by stacking surface SiO_2 -matrix overlays to suppress the leaching of the supported Mn cluster under the reaction conditions. Figure 1 shows schematics of the functionalization of the supported Mn clusters with surface SiO_2 -matrix overlays. A Mn_4O_2 precursor $[\text{Mn}_4\text{O}_2(\text{CH}_3\text{COO})_7(\text{bipy})_2](\text{ClO}_4) \cdot 3\text{H}_2\text{O}$ (1) was chemically attached on SiO_2 particles (Aerosil 200) (2), and subsequently SiO_2 -matrix overlays were stacked surrounding the supported Mn cluster by hydrolysis-polymerization of TMOS (5).

The attachment of $[\text{Mn}_4\text{O}_2(\text{CH}_3\text{COO})_7(\text{bipy})_2](\text{ClO}_4) \cdot 3\text{H}_2\text{O}$ (1) onto the surface of SiO_2 particles was performed by a wet impregnation method, and one of the CH_3COO ligands was observed to be reacted with surface Si-OH groups in the grafting process. Subsequent treatments under vacuum at different temperatures produced different supported Mn clusters (2, 3, and 4), whose structures were characterized by quantitative analysis of CH_3COO ligands, FT-IR, DR-UV/vis, and Mn K-edge XAFS. During the impregnation of 1 with SiO_2 , 0.9 equiv. of CH_3COOH to 1 was detected in a CH_2Cl_2 solution, and a SiO_2 -attached Mn cluster (2) was obtained. The amount of CH_3COO ligands remaining on 2 was observed to be 5.9 equiv. per 1 by a reaction with CF_3COOH , which was consistent with the released CH_3COOH ligand of 1.

Three broad FT-IR peaks of 2 attributed to $\nu(\text{CH}_3\text{COO})_{\text{sym}}$, $\nu(\text{CH}_3\text{COO})_{\text{asym}}$, and $\nu(\text{CH}_3\text{COO})$ of the CH_3COO ligands were observed at ~ 1420 , 1599 , and 1345 cm^{-1} , respectively,

which were similar to those of 1 (~ 1404 , ~ 1610 , and 1336 cm^{-1} , respectively) (Supporting Information, Figure S2 (A)). The shoulders shown on $\nu(\text{CH}_3\text{COO})_{\text{sym}}$ and $\nu(\text{CH}_3\text{COO})_{\text{asym}}$ peaks of 2 were lower than 1, suggesting the release of a CH_3COO ligand during the attachment. On the other hand, the release of bipy ligands of 1 was not observed during the first impregnation process. Three peaks attributed to the bipy ligands of 2 were observed by FT-IR at 1450 , 1472 , and 1500 cm^{-1} , which were similar to those of 1 (1448 , 1473 , and 1499 cm^{-1}) (Supporting Information, Figure S2 (A)). There was no significant change in the peak intensities of the three peaks attributed to bipy, indicating that the bipy ligands still coordinated to the Mn cluster on 2.

Two peaks attributed to the $\pi-\pi^*$ transition of the bipy ligands (234 and 294 nm) and two peaks attributed to the $d-\pi^*$ transition from Mn to the bipy ligands at 442 and 500 nm were observed in the transmittance UV/vis spectrum of 1 in CH_2Cl_2 (Figure 2). After the attachment of 1 to the SiO_2 surface, two characteristic peaks attributed to the $\pi-\pi^*$ transition of the bipy ligands were still observed at 242 and 303 nm , and two characteristic peaks in the visible region were also observed at 454 and 499 nm . There were no significant changes in the UV/vis region during the first impregnation step.

Edge energy at the Mn K-edge is considered to be relative to the actual oxidation state of Mn species, and the edge energy of the Mn species in 2 was observed to be 6550.4 eV , which was similar to that of 1 (6550.8 eV ; Supporting Information, Figure S3, Table S1). The formal oxidation states of four Mn ions were confirmed to be +3 by the ESI-TOF MS spectrum of 1 (Supporting Information, Figure S1). The local coordination structure of 2 was almost similar to that of 1 from Mn K-edge

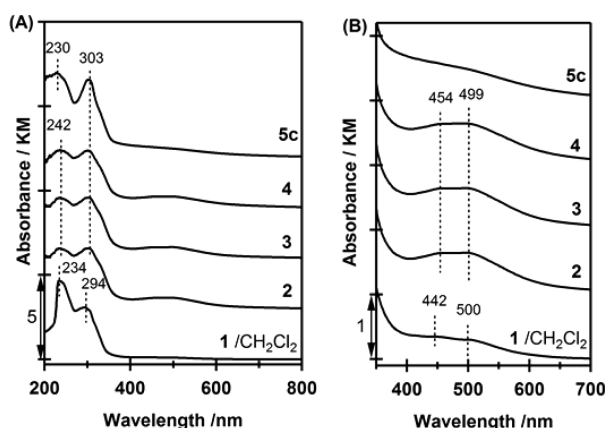


Figure 2. (A) UV/vis spectrum of **1** in CH₂Cl₂ and DR-UV/vis spectra of **2**, **3**, **4**, and **5c**. (B) Magnified view from 350 to 700 nm.

EXAFS (vide infra). Therefore, the Mn oxidation state of **2** was suggested to be +3.

The curve-fitting analysis of EXAFS suggested the local coordination structure of the SiO₂-supported Mn cluster (**2**) as shown in Table 1, Figure 3 and Supporting Information, Figure

Table 1. Structural Parameters of 1, 2, 3, and 5c Analyzed by Mn K-edge EXAFS Curve Fitting

shell	CN	R / nm	ΔE_0	$\sigma^2/10^5 \text{ nm}^2$
1: [Mn ₄ O ₂ (CH ₃ COO) ₇ (C ₁₀ H ₈ N ₂) ₂][ClO ₄ ·3H ₂ O] ^a				
Mn...Mn	0.5	0.287 ± 0.001	10 ± 1	2 ± 1
Mn...Mn	2	0.335 ± 0.001	10 ± 1	5 ± 1
Mn–O/N	3.9 ± 0.2	0.191 ± 0.001	8 ± 2	7 ± 1
Mn–O/N	2.1 ± 0.2	0.219 ± 0.001	8 ± 2	7 ± 1
2: SiO ₂ -supported Mn cluster (Mn: 2.2 wt %) ^b				
Mn...Mn	0.8 ± 1.0	0.285 ± 0.010	1 ± 18	5 ± 8
Mn...Mn	1.0 ± 1.2	0.335 ± 0.007	14 ± 12	4 ± 8
Mn–O/N	4.0 ± 2.4	0.189 ± 0.004	4 ± 7	8 ± 4
Mn–O/N	1.4 ± 2.4	0.220 ± 0.004	4 ± 7	8 ± 4
3: SiO ₂ -supported Mn cluster (Mn: 2.2 wt %) ^c				
Mn...Mn	1.3 ± 0.6	0.289 ± 0.003	5 ± 4	9 ± 4
Mn...Mn	0.9 ± 0.5	0.336 ± 0.003	17 ± 5	6 ± 4
Mn–O/N	2.7 ± 0.3	0.187 ± 0.001	3 ± 2	5 ± 1
5c: SiO ₂ -matrix functionalized Mn cluster (Mn: 0.7 wt %) ^d				
Mn...Mn	0.7 ± 0.3	0.301 ± 0.008	14 ± 11	9
Mn–O	1.4 ± 1.7	0.185 ± 0.006	3 ± 9	2 ± 8
Mn–O	1.0 ± 1.8	0.221 ± 0.013	14 ± 21	2 ± 8

^a $k = 30\text{--}140 \text{ nm}^{-1}$, $R = 0.09\text{--}0.34 \text{ nm}$, $R_f = 1.0\%$. S_0 was fitted to be 0.82. ^b $k = 30\text{--}120 \text{ nm}^{-1}$, $R = 0.08\text{--}0.34 \text{ nm}$, $R_f = 0.5\%$. $S_0 = 0.82$. ^c $k = 30\text{--}120 \text{ nm}^{-1}$, $R = 0.08\text{--}0.34 \text{ nm}$, $R_f = 0.4\%$. $S_0 = 0.82$. ^d $k = 30\text{--}110 \text{ nm}^{-1}$, $R = 0.07\text{--}0.30 \text{ nm}$, $R_f = 1.6\%$. $S_0 = 0.82$.

S4. Two peaks of Mn...Mn at 0.285 and 0.335 nm were observed on **2**. The contribution of the long Mn...Mn interaction decreased to half, while the short Mn...Mn interaction remained: two Mn...Mn interactions at $0.285 \pm 0.010 \text{ nm}$ (coordination number (CN) = 0.8 ± 1.0) and at $0.335 \pm 0.007 \text{ nm}$ (CN = 1.0 ± 1.2) were fitted, together with Mn–O(N) at $0.189 \pm 0.004 \text{ nm}$ (CN = 4.0 ± 2.4) and $0.220 \pm 0.004 \text{ nm}$ (CN = 1.4 ± 2.4). Similar UV/vis and Mn K-edge XANES spectra of **1** and **2** indicated that the coordination structure of the Mn cluster of **2** was similar to that of **1**. However, the structural parameters obtained by Mn K-edge EXAFS suggested that two Mn atoms at the edge position of

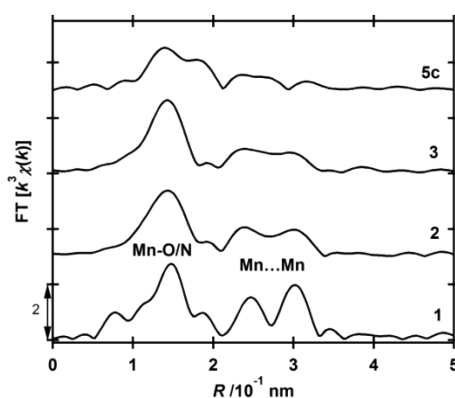


Figure 3. k^3 -Weighted Mn K-edge EXAFS Fourier transforms for **1**, **2**, **3**, and **5c**, measured at 20 K.

the Mn₄ butterfly framework of **1** stuck out, leading to the distortion of the Mn₄ cluster framework with the decrease in the CN of the long Mn–Mn interaction at 0.335 nm. A possible model of **2** is illustrated in Figure 1. The Mn–O–Mn bonds in **1** were negligible in Raman spectroscopy, as is the case in **2**.

We investigated further the treatment of **2** under vacuum at different temperatures to release extra CH₃COO ligands from the supported Mn complex. When **2** was heated at 373 K, in situ FT-IR measurements suggested that one of the six CH₃COO ligands on **2** was released, and the peak intensities attributed to the CH₃COO ligands remaining in **3** further decreased (Supporting Information, Figure S2(B)). The amount of CH₃COO ligands on **3** was estimated by GC to be 5.1 equiv relative to Mn₄. Further treatment under vacuum at 413 K produced **4** with 2.8 equiv of CH₃COO ligands relative to Mn₄. Mn K-edge XANES and EXAFS revealed that the Mn K-edge energy in **3** was similar to that in **2** (6550.5 eV; Supporting Information, Figure S3, Table S1); however, the CN of the Mn–O(N) interaction became smaller than that of **2** (Table 1). The edge energy suggested that the Mn oxidation state of **3** is +3. However, edge energy varies ($\sim 2 \text{ eV}$) when the coordination structures of metal complexes and the type of ligands are different even if they have the same formal oxidation states,³⁵ and it is difficult to conclude the details of the coordination structure of **3** from the obtained parameters from the curve-fitting analysis of EXAFS. The obvious fact is that bridging CH₃COO ligands were partially released by the heat treatment at 373 K (**3**), and the trend was enhanced at 413 K (**4**). DR-UV/vis spectra of **3** and **4** (Figure 2) showed two characteristic peaks in the visible region which were also observed at 454 and 499 nm, suggesting bipy ligands were still coordinated to the Mn center. It might be possible that other silanol groups coordinated from the surface to open coordination sites of the Mn cluster.

3-2. Surface Functionalization of SiO₂-Matrix Overlayers on the Surface of SiO₂ Particles Attaching the Mn Clusters. SiO₂-matrix overlayers were prepared on the SiO₂-supported Mn clusters (**2**) by CVD and subsequent hydrolysis–polymerization of tetramethoxysilane (TMOS) and H₂O. The stacking procedure and manner of the SiO₂-matrix overlayers on SiO₂ surfaces so as to surround supported metal complexes have previously been reported.³⁴ We prepared three SiO₂-matrix overlayers on **2** to produce three Mn catalysts (**5a**, **5b**, and **5c**). The SiO₂-matrix overlayers of **5a** were prepared by the hydrolysis–polymerization of TMOS in a step

using 0.67 g of TMOS and 0.27 mL of H₂O, respectively (for 0.2 g of **2**); that of **5b** was prepared using 1.34 g of TMOS and 0.54 mL of H₂O (twice amounts of **5a**), respectively, in one step CVD/hydrolysis–polymerization process. **5c** was prepared by performing the CVD/hydrolysis–polymerization processes twice, using 0.67 g of TMOS and 0.27 mL of H₂O, respectively, in each process. In the case of the hydrolysis–polymerization of TMOS for **5a**, almost 70% of the used TMOS was actually polymerized under the conditions.

Figure 4(A) shows ²⁹Si solid-state MAS NMR spectra of **5a**, **5b**, and **5c** with SiO₂-matrix overlayers, and three Si

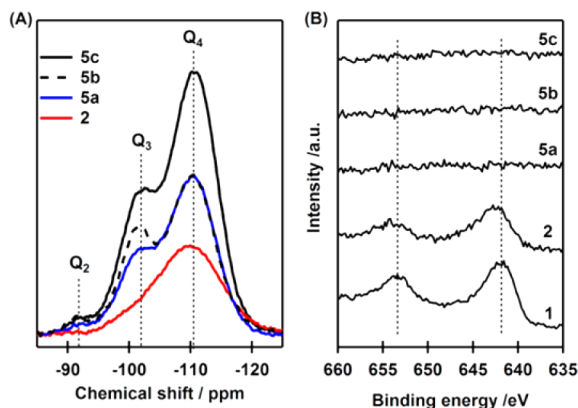


Figure 4. (A) ²⁹Si solid-state MAS NMR of **2**, **5a**, **5b**, and **5c**, and (B) Mn 2p XPS spectra of **1**, **2**, **5a**, **5b**, and **5c**.

components of Q₄ (Si(OSi)₄), Q₃ (Si(OSi)₃(OH)), and Q₂ (Si(OSi)₂(OH)₂) at around -111, -102, and -92 ppm, respectively, were observed. Difference between the spectra of **5** and **2** is attributed to Si species of the SiO₂-matrix overlayers of **5**, and the sum of areas of three Q₄, Q₃, and Q₂ peaks in a difference spectrum (**5** – **2**) is relative to the amount of stacked Si species by the hydrolysis–polymerization (Supporting Information, Figure S5). Although there is a possibility that the quantitative peak area analyses of ²⁹Si NMR spectra might be affected by paramagnetic Mn cluster complex (some Si sites might not be observed by ²⁹Si NMR), the effect of paramagnetic species was considered to be not significant in the current case since NMR of Mn₄ cluster (**1**) was measurable. The ratio of the sum of the peak areas of SiO₂-matrix overlayers on **5a**, **5b**, and **5c** was estimated to be 1/1.1/2.2. It was found that the repetition of the hydrolysis–polymerization cycles was efficient to increase the amount of SiO₂-matrix overlayers (**5c**), while the simple increase in the amounts of used TMOS and H₂O for the hydrolysis–polymerization process was inefficient (**5b**).

When 70% of used TMOS was polycondensed, the Si atomic ratio of the SiO₂-matrix overlayers to the SiO₂ support was 0.92. The Si atomic ratio calculated by using the peak intensities (the summation of the peak intensities of the three Si species) of ²⁹Si NMR in Figure 4A was 0.93, which agreed with the value calculated for mass gain. Assuming that the SiO₂-matrix overlayers spread on the surface of the SiO₂ support were of quartz structure, which exhibits the largest density of SiO₂, the calculated height of the observed amount of the SiO₂-matrix overlayers on **5a** was 2.2 nm on the used SiO₂ support (Aerosil 200; surface area: 200 m² g⁻¹). In the case of **5c**, the calculated height of the SiO₂-matrix overlayers was 4.3 nm. The average particle size of the SiO₂ support (Aerosil 200) was as

small as 12 nm and each SiO₂ particles gathered each other. It was difficult to estimate the actual average heights of the SiO₂-matrix overlayers by TEM. Transmission electron microscopy (TEM) revealed the morphological differences of **2** and **5c** (Figure 1(B) and Supporting Information, Figure S6). The surface of **5c** with the SiO₂-matrix overlayers was rougher after the stacking of SiO₂-matrix overlayers than that of **2**, and surface thin layers were observed as shown in Figure 1(B).

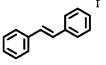
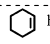
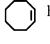

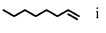
The ratios of the three Si species on **5c** were estimated to be 4% (Q₂), 34% (Q₃), and 62% (Q₄), respectively (Supporting Information, Figure S5). The major species being Q₄ indicated that Si–O–Si networks were formed by the hydrolysis–polymerization of TMOS. On the other hand, the Si species on **5b** were 10% (Q₂), 42% (Q₃), and 48% (Q₄), respectively. The amount of TMOS used for the hydrolysis–polymerization affected not only the amount of stacked SiO₂ matrix but also the ratio of these compositions.

Significant differences were also observed in the surface areas of **2**, **5a**, **5b**, and **5c**. N₂ adsorption isotherms at 77 K and their *t*-plots are presented in Supporting Information, Figure S7. The N₂ adsorption/desorption isotherms suggest increases in surface areas after the stacking of the SiO₂-matrix overlayers as well as the formation of micropores in the matrix overlayers. Brunauer–Emmett–Teller (BET) surface areas and external surface areas were respectively estimated to be 182 and 164 m² g⁻¹ for **2**, 347 and 286 m² g⁻¹ for **5a**, 578 and 529 m² g⁻¹ for **5b**, and 294 and 197 m² g⁻¹ for **5c**. Note that the external surface area of **5c** was similar to that of **2**, while the external surface areas of **5a** and **5b** were relatively higher than that of **2**. These results implied that the hydrolysis–polymerization produced a SiO₂ matrix with micropores and that repetition of the process tended to fill up the rough structures of the SiO₂ matrix, retaining the external surface area of the SiO₂ particles. The *t*-plot of **5c** had a gentle break at 0.37 nm, suggesting the formation of micropores with an average diameter of 0.74 nm.

Figure 4(B) shows Mn 2p_{3/2} and 2p_{1/2} XPS spectra of **2**, **5a**, **5b**, and **5c**. Mn 2p_{3/2} and 2p_{1/2} peaks for **1** were clearly observed at 641.7 and 653.4 eV, respectively, and those for **2** on SiO₂ were observed at 642.2 and 653.9 eV, respectively. The slight shifts in the Mn 2p binding energies would reflect the coordination of surface oxygen to the Mn complex. After the stacking of the SiO₂-matrix overlayers, the Mn 2p peaks were observed to get smaller. Even the Mn 2p peaks of **5a** entirely disappeared, as did those of **5b** and **5c** (Figure 4(B)). Considering the escape depth of Mn 2p, these results clearly indicated that the supported Mn clusters on the surface of the SiO₂ particles were closely surrounded by the produced SiO₂-matrix overlayers.

It was found out that the structure of **5c** after stacking of the SiO₂-matrix overlayers was different from that of **2**. Mn K-edge EXAFS found the local coordination structure of the supported Mn species on **5c**: Mn···Mn interaction length of 0.301 ± 0.008 nm (CN = 0.7 ± 0.3) and two Mn–O interactions at 0.185 ± 0.006 nm (CN = 1.4 ± 1.7) and 0.221 ± 0.013 nm (CN = 1.0 ± 1.8) (Table 1, Figure 3 and Supporting Information, Figure S4). The amount of remaining CH₃COO ligands of **5c** was estimated to be 2.0 equiv to Mn₄. In the DR-UV/vis spectrum of **5c**, the characteristic peaks attributed to d-π* transition from Mn to the bipy ligands disappeared (Figure 2 (B)). These results indicated that the partial release of the coordinating ligands brought about the transformation of the supported Mn cluster to dimeric Mn species in the SiO₂-matrix overlayers. Therefore, a possible composition of dimeric Mn species on **5c**

Table 2. Catalytic Performances of Mn Catalysts for Epoxidation of Alkenes^a

Entry	Catalyst	Reactant	Mn ₄ /Reactant/IBA	Time /h	Conversion % ^b	Selectivity % ^c	Leaching of Mn %/ ^d
1	--		0/500/1500	72	0	--	--
2	SiO ₂ ^e		0/500/1500	72	0	--	--
3	1		1/500/1500	4	97	94	--
4	2		1/500/1500	6	97	96	45.8
5	3		1/500/1500	6	99	96	53.4
6	4		1/500/1500	11	99	97	47.3
7	5a		1/500/1500	33	89	91	0.41
8	5b		1/500/1500	24	94	88	0.02
9	5c		1/500/1500	31	97	91	0.01
10	5c		1/500/0	72	0	0	--
11	5c ^g		1/500/1500	72	0	0	--
12	6		1/500/1500	12	99	97	38.6
13	7		1/500/1500	36	~0	n.d.	--
14	5c	 ^h	1/500/1500	15	92	82	--
15	5c	 ^h	1/500/1500	9	85	91	--
16	5c		1/500/1500	5.5	97	93	--
17	5c	 ⁱ	1/500/1500	9.5	46	55	--

^aReaction conditions: Mn₄, 0.67 × 10⁻⁶ mol; Mn₄/reactant/biphenyl/IBA = 1/500/250/1500; CH₂Cl₂, 3 mL; 283 K; O₂, 101.3 kPa. Biphenyl was used as an internal standard. ^bConversion % = (Initial mole of reactant – Residual mole of reactant)/Initial mole of reactant × 100%. ^cSelectivity % = Mole of epoxide product/(Initial mole of reactant – Residual mole of reactant) × 100%. ^dThe leaching of Mn was detected by ICP spectroscopy of the reaction mixture filtrate after the reaction. ^eThe amount of SiO₂ was 25 mg. ^fBenzaldehyde was formed as a byproduct. ^gThe reaction was conducted under N₂ atmosphere. ^hα,β-Unsaturated ketone was formed as a byproduct. ⁱ1-Heptanal and 3-octenone were formed as a byproduct. n.d.: not determined.

could be written as [Mn₂(CH₃COO)]₂, although the exact detailed structure was still controversial at this moment. The edge energy obtained from Mn K-edge XANES in **5c** (6548.7 eV; Supporting Information, Figure S3, Table S1) was smaller than that in **2**, suggesting the reduction of the Mn species.

3-3. Catalytic Performance in Alkene Epoxidation. Alkene epoxidation using O₂ and IBA (a sacrificial reagent)³³ was examined on the supported Mn clusters (**2–4** and **5a–c**). The results are summarized in Table 2. The homogeneous solution of **1** promoted the epoxidation of *trans*-stilbene with high selectivity of 94% (entry 3), whereas no reaction occurred without **1** (entry 1). The SiO₂-supported Mn clusters, **2–4**, showed activity and high selectivity over 95% (entries 4–6), whereas SiO₂ without Mn was inactive (entry 2). After a reaction was completed, the solid catalysts were separated from the solution phases, and the amounts of leached Mn species were determined by ICP measurements. It was found out that leaching of the supported Mn complexes was substantial: 45.8% for **2**, 53.4% for **3**, and 47.3% for **4**. These results suggested that these supported Mn clusters that were simply attached to the surface were not durable under heterogeneous epoxidation conditions.

The preparation of the SiO₂-matrix overlayers on the SiO₂-supported Mn clusters imparted the catalyst with remarkable stability (Table 2). The supported Mn catalysts with the SiO₂-matrix overlayers (**5a**, **5b**, and **5c**) promoted the epoxidation with high selectivity for *trans*-stilbene epoxide: 91% for **5a**, 88%

for **5b**, and 91% for **5c** at ~90% conversion for 24–33 h (entries 7–9). Although the epoxidation reaction became slower, the leaching of the active Mn catalyst was significantly suppressed on **5a–c**. The amounts of leached Mn species were 0.41% for **5a** and negligible for **5b** (0.02%) and **5c** (0.01%). When the reaction was run to a conversion of ~50%, the reaction solution was filtered from solid **5c** and showed no further progress in the catalytic reaction (Figure 5(A)). On the other hand, the filtration of **3** was significantly active. These results clearly show that the supported Mn catalysts embedded in the SiO₂-matrix overlayers, in particular **5c**, were highly stable, and that the catalytic reaction on **5c** proceeded in the heterogeneous phase without unfavorable leaching of Mn into solution. In contrast, dissolved Mn in the solution was active on **3**. After the 500 cycle of epoxidation, no Mn–Mn interaction was observed on **5c** (Supporting Information, Figure S4 and Table S2). The decrease in the amount of Mn in the catalyst was not observed during the reaction, suggesting that transient leaching and re-deposition of the Mn species would not contribute to the reaction.³⁶

Figures 5(B), 5(C), and Supporting Information, Figure S8 show the conversion of *trans*-stilbene, the selectivity of *trans*-stilbene oxide, and the amount of Mn species remaining on the SiO₂ particle surface on the catalysts **3** and **5c** after they were recycled 5 times. On **3** without the SiO₂-matrix overlayers, the conversion decreased significantly because of the extensive leaching of Mn species into solution. After 2 cycles of

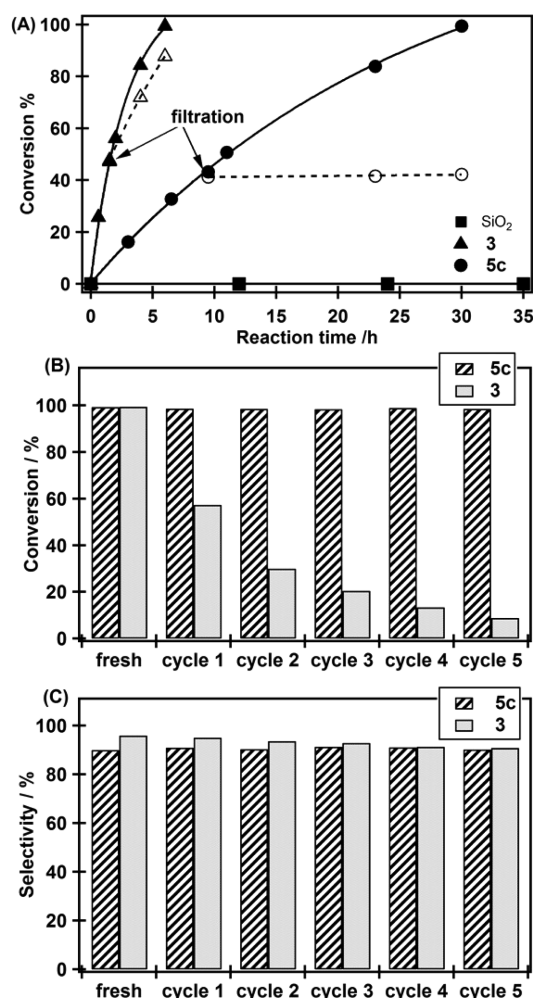


Figure 5. (A) Test of the heterogeneous nature of the catalysts in *trans*-stilbene epoxidation. ((B), (C)) Recycling tests of 3 (for 6 h) and 5c (for 30 h) in *trans*-stilbene epoxidation. (B) Conversion of each cycle; (C) selectivity for epoxide; reaction conditions: Mn₄, 0.67 × 10⁻⁶ mol; Mn₄/*trans*-stilbene/IBA = 1/500/1500; CH₂Cl₂, 3 mL; 283 K; O₂, 101.3 kPa.

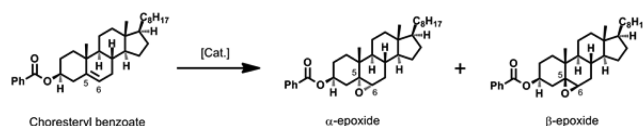
epoxidation, 80% of the supported Mn clusters were lost (Supporting Information, Figure S8). On the other hand, the leaching of the Mn catalyst on 5c with the SiO₂-matrix overlayers was negligible after 6 epoxidation cycles, and the conversion of *trans*-stilbene remained >90%, keeping up with the high epoxide selectivity. The differences were obvious between 3 and 5c, demonstrating the positive effect of the surface SiO₂-matrix overlayers on the stability of the supported Mn epoxidation catalysts.

Other alkenes were smoothly converted to epoxides on 5c (Table 2). Observed major byproducts were aldehydes from C=C bond cleavage and ketones from oxidation at the α -position. The reactions of internal alkenes such as cyclohexene, cyclooctene, and norbornene produced epoxides with high selectivity, whereas the selectivity of terminal alkene such as 1-octene was low, forming 1-heptanal and 3-octenone as byproducts.

We also investigated the epoxidation of cholesteryl benzoate using *m*-chloroperbenzoic acid (*m*-CPBA) and the Mn catalyst 5c. The experiment suggests whether a Mn center contributes to the oxidation step in epoxidation cycle or not.^{33a} The epoxidation of cholesteryl benzoate provides two epoxide

products, α -epoxide and β -epoxide (Scheme 1). In the case of autoxidation using peroxy species (e.g., *m*-CPBA), α -epoxide is

Scheme 1. Epoxidation of Cholesteryl Benzoate



preferably produced. Analogously, if a free peroxy species were to be formed on the Mn site, but reacted independently with an alkene reactant in solution (in a similar way as autoxidation), the selective formation of α -epoxide would also be observed. On the other hand, if the epoxidation step were to proceed on a metal site, the steric hindrance between the cholesteryl benzoate at 5 and 6-position and the metal center is expected to change the selectivity of the products. It was reported that the selectivity of the cholesteryl benzoate epoxidation changed (β -epoxide was preferably obtained) when catalytic amounts of Mn(II) complexes were used in the O₂/IBA system.^{33a} For instance, the α -epoxide/ β -epoxide product ratio on bis-(acetylacetonato)manganese(II) was reported to be 20/80 and that on bis(dipivaloylmethanato)manganese(II) was 18/82.^{33a}

We performed the epoxidation of the cholesteryl benzoate with *m*-CPBA and 5c. With *m*-CPBA without the Mn catalysts, the α -epoxide was preferably formed with the α -epoxide/ β -epoxide product ratio of 73/27 (6.5 h; determined by ¹H NMR), which agreed with reported results.^{33a} On the other hand, the product ratio of α -epoxide/ β -epoxide was 20/80 (24 h) on 5c. The reaction mechanism and intermediate structures on 5c are not clear at the moment, but the opposite epoxide selectivity for the epoxidation of the cholesteryl benzoate suggests that the Mn species on 5c surrounded by the SiO₂-matrix overlayers indeed are involved in the epoxidation step.

It is to be noted that the activation energy of catalytic epoxidation on 5c differed widely by alkene. Cyclooctene epoxidation had similar activation energies on 3 (15 kJ mol⁻¹) and 5c (16 kJ mol⁻¹), and the turnover frequencies (TOFs) were 4.0 × 10⁻² and 1.9 × 10⁻² s⁻¹, respectively. On the other hand, the TOFs and activation energies for the epoxidation of the larger reactant *trans*-stilbene on 5c were 6.7 × 10⁻³ s⁻¹ and 31 kJ mol⁻¹, whereas those on 3 were 2.5 × 10⁻² s⁻¹ and 15 kJ mol⁻¹. The small activation energies around 15 kJ mol⁻¹ on 3 might be related to mass transfer. The smaller reaction rate of *trans*-stilbene on 5c is due to the diffusion resistance of the reactants inside the SiO₂-matrix overlayers. The 2-fold higher activation energies for the *trans*-stilbene epoxidation on 5c would result from the different transition state structure produced from the reactant, the oxidant, and the Mn species on 5c inside the SiO₂-matrix overlayers. Since the structure of Mn species on 5c was totally different from that on 3, the loss of CH₃COO and bipy ligands, the addition of surface silanol groups, and the existence of SiO₂-matrix overlayers, the structures of transition state and intermediate responsible for determining activation energy would be different. The steric hindrance for the coordination and subsequent oxidation of *trans*-stilbene at the Mn site inside the surface-matrix overlayers would also be one of the reasons to produce the different transition state/intermediate structures.^{34a} Similar trends were observed for the cholesteryl benzoate epoxidation (14 kJ mol⁻¹ on 3; 74 kJ mol⁻¹ on 5c), supporting the above discussion.

We also prepared catalyst **6** by releasing the ligands of **2** at 673 K so that **6** had MnO_x as supported species. Catalyst **7** was prepared by subsequent stacking of SiO_2 -matrix overlayers on **6** with MnO_x species. It is to be noted that **6** and **7** exhibited different epoxidation performances as shown in Table 2. Catalyst **6** exhibited a similar behavior to catalysts **2**, **3**, and **4** (conversion: 99%, epoxide selectivity: 97%) for the *trans*-stilbene epoxidation, and significant leaching was observed (38.6% for 12 h) (entry 12). On the contrary, the epoxidation was suppressed on **7**, and the corresponding epoxide was not observed even after 36 h (entry 13). These results suggested that the stacking of the SiO_2 -matrix overlayers on the MnO_x species without the coordinating ligands did not provide reaction space above the Mn site, resulting in large loss of the catalytic activity.

Although the coordination structure of **5c** decomposed from the Mn_4 clusters (**1** and **2**) during the preparation step of the SiO_2 -matrix overlayers, the catalyst **5c** prepared on **2** with the Mn cluster with the several coordinating ligands cannot be obtained from the simple supported MnO_x species on the SiO_2 surface. Indeed, **5c**, whose complete local coordination structure is not clear at the moment, exhibited robust epoxidation performances under the identical conditions. The integration of the active Mn site and the surface SiO_2 -matrix overlayers would cooperatively achieve robust catalysis in the heterogeneous phase.

4. CONCLUSIONS

The functionalization of the surface of SiO_2 particles with attached $[\text{Mn}_4\text{O}_2(\text{CH}_3\text{COO})_7(\text{bipy})_2](\text{ClO}_4)\cdot 3\text{H}_2\text{O}$ (**1**) and the stacking of SiO_2 -matrix overlayers were successfully used to prepare a new and robust heterogeneous Mn catalyst for the selective epoxidation of alkenes. **1** was chemically attached to a SiO_2 particle surface, and the attached structure was characterized by FT-IR, UV/vis, Raman spectroscopy, XPS, and Mn K-edge XAFS. The stacking of surface SiO_2 -matrix overlayers surrounding the supported Mn clusters of **2** with a similar structure to the precursor **1** brought about a structural change in the original Mn cluster to an active dimeric Mn species on **5c** together with the formation of a reaction space in the close proximity of the Mn species inside the SiO_2 -matrix overlayers. **5c** exhibited different catalytic activity, especially in the reaction rate and activation energy compared with **2** and **3**, and the durability of the Mn catalysts under the epoxidation reaction conditions was remarkably improved. The leaching of the supported Mn catalysts on **5c** was prevented. The surface functionalization through the SiO_2 -matrix overlayers to provide the composite of an active metal site and a reaction space is promising to achieve a robust catalysis on a supported metal catalyst in a heterogeneous phase.

■ ASSOCIATED CONTENT

Supporting Information

An ESI-TOM MS spectrum, FT-IR spectra, Mn K-edge XANES and EXAFS spectra and their analyses, ^{29}Si NMR spectra, N_2 adsorption, TEM images, and residual Mn ratio in recycling tests. This material is available free of charge via the Internet at <http://pubs.acs.org>.

■ AUTHOR INFORMATION

Corresponding Author

*E-mail: smura@ims.ac.jp (S.M.), mtada@ims.ac.jp (M.T.).

Notes

The authors declare no competing financial interest.

■ ACKNOWLEDGMENTS

The authors thank Prof. Kentaro Tanaka and Prof. Yasuyuki Yamada at Nagoya University for measuring the ESI-TOF MS spectrum of **1**. This work was supported by the JSPS Funding Program for Next Generation World-Leading Researchers (GR090), MEXT/JSPS KAKENHI Grants Nos. 22108534 and 23750068, NEDO, and JST Research Seeds Program. XAFS measurements were performed with the approval of PF-PAC (Nos. 2010G021 and 2011G176).

■ REFERENCES

- (1) (a) Shibasaki, M.; Yamamoto, Y., Eds.; *Multimetallic Catalysts in Organic Synthesis*; Wiley-VCH Verlag GmbH & Co. KGaA: Weinheim, Germany, 2004. (b) Christmann, M.; Bräse, S., Eds.; *Asymmetric Synthesis—The Essentials*; Wiley-VCH Verlag GmbH & Co. KGaA: Weinheim, Germany, 2007.
- (2) Reviews for supported metal complex catalysts are as follows: (a) Sheldon, R. A.; Wallau, M.; Arends, I. W. C. E.; Schuchardt, U. *Acc. Chem. Res.* **1998**, *31*, 485–493. (b) McMorn, P.; Hutchings, G. J. *Chem. Soc. Rev.* **2004**, *33*, 108–122. (c) Thomas, J. M.; Raja, R.; Lewis, D. W. *Angew. Chem., Int. Ed.* **2005**, *44*, 6456–6482. (d) Notestein, J. M.; Katz, A. *Chem.—Eur. J.* **2006**, *12*, 3954–3965. (e) Corma, A.; García, H. *Adv. Synth. Catal.* **2006**, *348*, 1391–1412. (f) Tada, M.; Iwasawa, Y. *Chem. Commun.* **2006**, 2833–2844. (g) Copéret, C.; Basset, J.-M. *Adv. Synth. Catal.* **2007**, *349*, 78–92. (h) Wegener, S. L.; Marks, T. J.; Stair, P. C. *Acc. Chem. Res.* **2012**, *45*, 206–214.
- (3) Examples for supported metal complex catalysts are as follows: (a) Tada, M.; Shimamoto, M.; Sasaki, T.; Iwasawa, Y. *Chem. Commun.* **2004**, 2562–2563. (b) Le Roux, E.; Chabanas, M.; Baudouin, A.; de Mallmann, A.; Copéret, C.; Quadrelli, E. A.; Thivolle-Cazat, J.; Basset, J.-M.; Lukens, W.; Lesage, A.; Emsley, L.; Sunley, G. J. *J. Am. Chem. Soc.* **2004**, *126*, 13391–13399. (c) Rioulet, V.; Quadrelli, E. A.; Copéret, C.; Basset, J.-M.; Andersen, R. A.; Köhler, K.; Böttcher, R.-M.; Herdtweck, E. *Chem.—Eur. J.* **2005**, *11*, 7358–7365. (d) Rendón, N.; Berthoud, R.; Blanc, F.; Gajan, D.; Maishal, T.; Basset, J.-M.; Copéret, C.; Lesage, A.; Emsley, L.; Marinescu, S. C.; Singh, R.; Schrock, R. R. *Chem.—Eur. J.* **2009**, *15*, 5083–5089. (e) Villaverde, G.; Corma, A.; Iglesias, M.; Sánchez, F. *ChemCatChem* **2011**, *3*, 1320–1328. (f) Goodrich, P.; Hardacre, C.; Paun, C.; Ribeiro, A.; Kennedy, S.; Lourenço, M. J. V.; Manyar, H.; Nieto de Castro, C. A.; Besnea, M.; Pârvulescu, V. I. *Adv. Synth. Catal.* **2011**, *353*, 995–1004. (g) Sievers, C.; Jiménez, O.; Knapp, R.; Lin, X.; Müller, T. E.; Türlér, A.; Wierczinski, B.; Lercher, J. A. *J. Mol. Catal. A: Chem.* **2008**, *279*, 187–199. (h) Caplan, N. A.; Hancock, F. E.; Bulman Page, P. C.; Hutchings, G. J. *Angew. Chem., Int. Ed.* **2004**, *43*, 1685–1688. (i) Hara, K.; Akiyama, R.; Takakusagi, S.; Uosaki, K.; Yoshino, T.; Kagi, H.; Sawamura, M. *Angew. Chem., Int. Ed.* **2008**, *47*, 5627–5630. (j) Tada, M.; Coquet, R.; Yoshida, J.; Kinoshita, M.; Iwasawa, Y. *Angew. Chem., Int. Ed.* **2007**, *46*, 7220–7223. (k) Tada, M.; Akatsuka, Y.; Yang, Y.; Sasaki, T.; Kinoshita, M.; Motokura, K.; Iwasawa, Y. *Angew. Chem., Int. Ed.* **2008**, *47*, 9252–9255. (l) Tada, M.; Muratsugu, S.; Kinoshita, M.; Sasaki, T.; Iwasawa, Y. *J. Am. Chem. Soc.* **2010**, *132*, 713–724. (m) Muratsugu, S.; Weng, Z.; Nakai, H.; Isobe, K.; Kushida, Y.; Sasaki, T.; Tada, M. *Phys. Chem. Chem. Phys.* **2012**, *14*, 16023–16031.
- (4) (a) Brinksma, J.; de Boer, J. W.; Hage, R.; Feringa, B. L. In *Modern Oxidation Methods*; Bäckvall, J.-E., Ed.; Wiley-VCH Verlag GmbH & Co. KGaA: Weinheim, Germany, 2004; pp 295–326. (b) Dismukes, G. C.; Brimblecombe, R.; Felton, G. A. N.; Pryadun, R. S.; Sheats, J. E.; Spiccia, L.; Swiegers, G. F. *Acc. Chem. Res.* **2009**, *42*, 1935–1943.
- (5) (a) Collman, J. P.; Lee, V. J.; Kellen-Yuen, C. J.; Zhang, X.; Ibers, J. A.; Brauman, J. I. *J. Am. Chem. Soc.* **1995**, *117*, 692–703. (b) Shimazaki, Y.; Nagano, T.; Takesue, H.; Ye, B.-H.; Tani, F.; Naruta, Y. *Angew. Chem., Int. Ed.* **2004**, *43*, 98–100. (c) Rebelo, S. L.

- H.; Pereira, M. M.; Simões, M. M. Q.; Neves, M. G. P. M. S.; Cavaleiro, J. A. S. *J. Catal.* **2005**, *234*, 76–87. (d) Srour, H.; Le Maux, P.; Simonneaux, G. *Inorg. Chem.* **2012**, *51*, 5850–5856.
- (6) (a) Irie, R.; Noda, K.; Ito, Y.; Matsumoto, N.; Katsuki, T. *Tetrahedron Lett.* **1990**, *31*, 7345–7348. (b) Zhang, W.; Loebach, J. L.; Wilson, S. R.; Jacobsen, E. N. *J. Am. Chem. Soc.* **1990**, *112*, 2801–2803. (c) Kureshy, R. I.; Khan, N. H.; Abdi, S. H. R.; Singh, S.; Ahmed, I.; Shukla, R. S.; Jasra, R. V. *J. Catal.* **2003**, *219*, 1–7. (d) Shitama, H.; Katsuki, T. *Chem.—Eur. J.* **2007**, *13*, 4849–4858. (e) Zhang, J.-L.; Garner, D. K.; Liang, L.; Barrios, D. A.; Lu, Y. *Chem.—Eur. J.* **2009**, *15*, 7481–7489.
- (7) (a) Wieghardt, K.; Bossek, U.; Nuber, B.; Weiss, J.; Bonvoisin, J.; Corbella, M.; Vitols, S. E.; Girerd, J. J. *J. Am. Chem. Soc.* **1988**, *110*, 7398–7411. (b) Hage, R.; Iburg, J. E.; Kerschner, J.; Koek, J. H.; Lempers, E. L. M.; Martens, R. J.; Racherla, U. S.; Russell, S. W.; Swarthoff, T.; van Vliet, M. R. P.; Warnaar, J. B.; van der Wolf, L.; Krijnen, B. *Nature* **1994**, *369*, 637–639. (c) Quee-Smith, V. C.; DelPizzo, L.; Jureller, S. H.; Kerschner, J. L.; Hage, R. *Inorg. Chem.* **1996**, *35*, 6461–6465. (d) De Vos, D.; Bein, T. *Chem. Commun.* **1996**, 917–918. (e) De Vos, D. E.; Sels, B. F.; Reynaers, M.; Subba Rao, Y. V.; Jacobs, P. A. *Tetrahedron Lett.* **1998**, *39*, 3221–3224. (f) De Vos, D. E.; de Wildeman, S.; Sels, B. F.; Grobet, P. J.; Jacobs, P. A. *Angew. Chem., Int. Ed.* **1999**, *38*, 980–983. (g) Burdinski, D.; Bothe, E.; Wieghardt, K. *Inorg. Chem.* **2000**, *39*, 105–116. (h) de Boer, J. W.; Brinksma, J.; Browne, W. R.; Meetsma, A.; Alsters, P. L.; Hage, R.; Feringa, B. L. *J. Am. Chem. Soc.* **2005**, *127*, 7990–7991. (i) de Boer, J. W.; Browne, W. R.; Brinksma, J.; Alsters, P. L.; Hage, R.; Feringa, B. L. *Inorg. Chem.* **2007**, *46*, 6353–6372. (j) de Boer, J. W.; Alsters, P. L.; Meetsma, A.; Hage, R.; Browne, W. R.; Feringa, B. L. *Dalton Trans.* **2008**, 6283–6295.
- (8) (a) Yagi, M.; Wolf, K. V.; Baesjou, P. J.; Bernasek, S. L.; Dismukes, G. C. *Angew. Chem., Int. Ed.* **2001**, *40*, 2925–2928. (b) Brimblecombe, R.; Swiegers, G. F.; Dismukes, G. C.; Spiccia, L. *Angew. Chem., Int. Ed.* **2008**, *47*, 7335–7338.
- (9) (a) Kanyo, Z. F.; Scolnick, L. R.; Ash, D. E.; Christianson, D. W. *Nature* **1996**, *383*, 554–557. (b) Boelrijk, A. E. M.; Dismukes, G. C. *Inorg. Chem.* **2000**, *39*, 3020–3028. (c) Wu, A. J.; Penner-Hahn, J. E.; Pecoraro, V. L. *Chem. Rev.* **2004**, *104*, 903–938. (d) Jackson, T. A.; Brunold, T. C. *Acc. Chem. Res.* **2004**, *37*, 461–470.
- (10) (a) Yagi, M.; Kaneko, M. *Chem. Rev.* **2001**, *101*, 21–35. (b) Mukhopadhyay, S.; Mandal, S. K.; Bhaduri, S.; Armstrong, W. H. *Chem. Rev.* **2004**, *104*, 3981–4026. (c) Yano, J.; Yachandra, V. K. *Inorg. Chem.* **2008**, *47*, 1711–1726. (d) Pushkar, Y.; Long, X.; Glatzel, P.; Brudvig, G. W.; Dismukes, G. C.; Collins, T. J.; Yachandra, V. K.; Yano, J.; Bergmann, U. *Angew. Chem., Int. Ed.* **2010**, *49*, 800–803. (e) Umena, Y.; Kawakami, K.; Shen, J.-R.; Kamiya, N. *Nature* **2011**, *473*, 55–61.
- (11) (a) Zondervan, C.; Hage, R.; Feringa, B. L. *Chem. Commun.* **1997**, 419–420. (b) Carrell, T. G.; Cohen, S.; Dismukes, G. C. *J. Mol. Catal. A: Chem.* **2002**, *187*, 3–15.
- (12) (a) Kang, B.; Kim, M.; Lee, J.; Do, Y.; Chang, S. J. *Org. Chem.* **2006**, *71*, 6721–6727. (b) Kilic, H.; Adam, W.; Alsters, P. L. *J. Org. Chem.* **2009**, *74*, 1135–1140.
- (13) Barker, J. E.; Ren, T. *Tetrahedron Lett.* **2004**, *45*, 4681–4683.
- (14) Bennur, T. H.; Sabne, S.; Deshpande, S. S.; Srinivas, D.; Sivasanker, S. *J. Mol. Catal. A: Chem.* **2002**, *185*, 71–80.
- (15) (a) Knops-Gerrits, P.-P.; De Vos, D.; Thibault-Starzyk, F.; Jacobs, P. A. *Nature* **1994**, *369*, 543–546. (b) Sabater, M. J.; Corma, A.; Domenech, A.; Fornés, V.; García, H. *Chem. Commun.* **1997**, 1285–1286. (c) Alcón, M. J.; Corma, A.; Iglesias, M.; Sánchez, F. J. *Mol. Catal. A: Chem.* **2002**, *178*, 253–266. (d) Chavan, S. A.; Srinivas, D.; Ratnasamy, P. *J. Catal.* **2002**, *212*, 39–45.
- (16) (a) Serrano, D. P.; Aguado, J.; Vargas, C. *Appl. Catal., A* **2008**, *335*, 172–179. (b) Saikia, L.; Srinivas, D. *Catal. Today* **2009**, *141*, 66–71.
- (17) (a) Kureshy, R. I.; Khan, N. H.; Abdi, S. H. R.; Ahmad, I.; Singh, S.; Jasra, R. V. *J. Catal.* **2004**, *221*, 234–240. (b) Kuźniarska-Biernacka, I.; Silva, A. R.; Ferreira, R.; Carvalho, A. P.; Pires, J.; de Carvalho, M. B.; Freire, C.; de Castro, B. *New. J. Chem.* **2004**, *28*, 853–858.
- (c) Kuźniarska-Biernacka, I.; Silva, A. R.; Carvalho, A. P.; Pires, J.; Freire, C. *Langmuir* **2005**, *21*, 10825–10834. (d) Cardoso, M.; Silva, A. R.; de Castro, B.; Freire, C. *Appl. Catal., A* **2005**, *285*, 110–118.
- (18) (a) Bhattacharjee, S.; Anderson, J. A. *Chem. Commun.* **2004**, 554–555. (b) Bhattacharjee, S.; Dines, T. J.; Anderson, J. A. *J. Catal.* **2004**, *225*, 398–407. (c) Bhattacharjee, S.; Anderson, J. A. *Adv. Synth. Catal.* **2006**, *348*, 151–158.
- (19) Silva, A. R.; Vital, J.; Figueiredo, J. L.; Freire, C.; de Castro, B. *New. J. Chem.* **2003**, *27*, 1511–1517.
- (20) (a) Bigi, F.; Moroni, L.; Maggi, R.; Sartori, G. *Chem. Commun.* **2002**, 716–717. (b) Zhang, H.; Xiang, S.; Xiao, J.; Li, C. *J. Mol. Catal. A: Chem.* **2005**, *238*, 175–184. (c) Zhang, H.; Wang, Y. M.; Zhang, L.; Gerritsen, G.; Abbenhuis, H. C. L.; van Santen, R. A.; Li, C. *J. Catal.* **2008**, *256*, 226–236. (d) Jutz, F.; Grunwaldt, J.-D.; Baiker, A. *J. Mol. Catal. A: Chem.* **2008**, *279*, 94–103.
- (21) (a) Terry, T. J.; Stack, T. D. P. *J. Am. Chem. Soc.* **2008**, *130*, 4945–4953. (b) Tang, J.; Zu, Y.; Huo, W.; Wang, L.; Wang, J.; Jia, M.; Zhang, W.; Thiel, W. R. *J. Mol. Catal. A: Chem.* **2012**, *355*, 201–209.
- (22) (a) Schoenfeldt, N. J.; Korinda, A. W.; Notestein, J. M. *Chem. Commun.* **2010**, 46, 1640–1642. (b) Schoenfeldt, N. J.; Ni, Z.; Korinda, A. W.; Meyer, R. J.; Notestein, J. M. *J. Am. Chem. Soc.* **2011**, *133*, 18684–18695. (c) Schoenfeldt, N. J.; Notestein, J. M. *ACS Catal.* **2011**, *1*, 1691–1701.
- (23) (a) Song, C. E.; Roh, E. J.; Yu, B. M.; Chi, D. Y.; Kim, S. C.; Lee, K.-J. *Chem. Commun.* **2000**, 615–616. (b) Nielsen, M.; Thomsen, A. H.; Jensen, T. R.; Jakobsen, H. J.; Skibsted, J.; Gothelf, K. V. *Eur. J. Org. Chem.* **2005**, 342–347. (c) Amarasekara, A. S.; McNeal, I.; Murillo, J.; Green, D.; Jennings, A. *Catal. Commun.* **2008**, *9*, 2437–2440.
- (24) Tan, R.; Yin, D.; Yu, N.; Zhao, H.; Yin, D. *J. Catal.* **2009**, *263*, 284–291.
- (25) (a) Cho, S.-H.; Ma, B.; Nguyen, S. T.; Hupp, J. T.; Albrecht-Schmitt, T. E. *Chem. Commun.* **2006**, 2563–2565. (b) Cho, S.-H.; Gadzikwa, T.; Afshari, M.; Nguyen, S. T.; Hupp, J. T. *Eur. J. Inorg. Chem.* **2007**, 4863–4867. (c) Song, F.; Wang, C.; Falkowski, J. M.; Ma, L.; Lin, W. *J. Am. Chem. Soc.* **2010**, *132*, 15390–15398. (d) Bhattacharjee, S.; Yang, D.-A.; Ahn, W.-S. *Chem. Commun.* **2011**, 47, 3637–3639.
- (26) (a) Vincent, J. B.; Christmas, C.; Chang, H. R.; Li, Q.; Boyd, P. D. W.; Huffman, J. C.; Hendrickson, D. N.; Christou, G. *J. Am. Chem. Soc.* **1989**, *111*, 2086–2097. (b) Christou, G. *Acc. Chem. Res.* **1989**, *22*, 328–335. (c) Tamane, T.; Tsubomura, T.; Sakai, K. *Acta Crystallogr.* **1996**, *C52*, 777–779.
- (27) (a) Libby, E.; McCusker, J. K.; Schmitt, E. A.; Folting, K.; Hendrickson, D. N.; Christou, G. *Inorg. Chem.* **1991**, *30*, 3486–3495. (b) Wemple, M. W.; Tsai, H.-L.; Wang, S.; Claude, J. P.; Streib, W. E.; Huffman, J. C.; Hendrickson, D. N.; Christou, G. *Inorg. Chem.* **1996**, *35*, 6437–6449. (c) Albela, B.; El Fallah, M. S.; Ribas, J.; Folting, K.; Christou, G.; Hendrickson, D. N. *Inorg. Chem.* **2001**, *40*, 1037–1044. (d) Karotsis, G.; Jones, L. F.; Papaefstathiou, G. S.; Collins, A.; Parsons, S.; Nguyen, T. D.; Evangelisti, M.; Brechin, E. K. *Dalton Trans.* **2008**, 4917–4925.
- (28) Vincent, J. B.; Chang, H.-R.; Folting, K.; Huffman, J. C.; Christou, G.; Hendrickson, D. N. *J. Am. Chem. Soc.* **1987**, *109*, 5703–5711.
- (29) (a) Ravel, B.; Newville, M. *J. Synchrotron Rad.* **2005**, *12*, 537–541. (b) Newville, M.; Ravel, B.; Haskel, D.; Rehr, J. J.; Stern, E. A.; Yacoby, Y. *Phys. B* **1995**, *208–209*, 154–156.
- (30) Thompson, A.; Attwood, D.; Gullikson, E.; Howells, M.; Kim, K.-J.; Kirz, J.; Kortright, J.; Lindau, I.; Liu, Y.; Pianetta, P.; Robinson, A.; Scofield, J.; Underwood, J.; Williams, G.; Winick, H. *X-ray Data Booklet*; Lawrence Berkeley National Laboratory, University of California: Berkeley, CA, 2009.
- (31) Newville, M.; Liviš, P.; Yacoby, Y.; Rher, J. J.; Stern, E. A. *Phys. Rev. B* **1993**, *47*, 14126–14131.
- (32) Ankudinov, A. L.; Ravel, B.; Rehr, J. J.; Conradson, S. D. *Phys. Rev. B* **1998**, *58*, 7565–7576.
- (33) (a) Yamada, T.; Imagawa, K.; Mukaiyama, T. *Chem. Lett.* **1992**, 2109–2112. (b) Haber, J.; Młodnicka, T.; Poltowicz, J. *J. Mol. Catal.*

- 1989, 54, 451–461. (c) Rodgers, K. R.; Arafa, I. M.; Goff, H. M. *J. Chem. Soc., Chem. Commun.* **1990**, 1323–1324. (d) Yamada, T.; Takai, T.; Rhode, O.; Mukaiyama, T. *Chem. Lett.* **1991**, 1–4. (e) Takai, T.; Hata, E.; Yamada, T.; Mukaiyama, T. *Bull. Chem. Soc. Jpn.* **1991**, 64, 2513–2518. (f) Murahashi, S.-I.; Oda, Y.; Naota, T. *J. Am. Chem. Soc.* **1992**, 114, 7913–7914. (g) Mukaiyama, T.; Yamada, T.; Nagata, T.; Imagawa, K. *Chem. Lett.* **1993**, 327–330. (h) Imagawa, K.; Nagata, T.; Yamada, T.; Mukaiyama, T. *Chem. Lett.* **1994**, 527–530. (i) Kaneda, K.; Ueno, S.; Imanaka, T. *J. Mol. Catal. A: Chem.* **1995**, 102, 135–138.
- (34) (a) Tada, M.; Sasaki, T.; Iwasawa, Y. *Phys. Chem. Chem. Phys.* **2002**, 4, 4561–4574. (b) Tada, M.; Sasaki, T.; Iwasawa, Y. *J. Catal.* **2002**, 211, 496–510. (c) Tada, M.; Sasaki, T.; Shido, T.; Iwasawa, Y. *Phys. Chem. Chem. Phys.* **2002**, 4, 5899–5909. (d) Tada, M.; Sasaki, T.; Iwasawa, Y. *J. Phys. Chem. B* **2004**, 108, 2918–2930. (e) Yang, Y.; Weng, Z.; Muratsugu, S.; Ishiguro, N.; Ohkoshi, S.; Tada, M. *Chem.—Eur. J.* **2012**, 18, 1142–1153. (f) Muratsugu, S.; Tada, M. *Acc. Chem. Res.* **2013**, 46, 300–311.
- (35) (a) Sauer, K.; Yachandra, V. K.; Britt, R. D.; Klein, M. P. In *Manganese Redox Enzymes*; Pecoraro, V. L., Ed.; VCH: New York, 1992; Chapter 8. (b) Penner-Hahn, J. E.; Fronko, R. M.; Pecoraro, V. L.; Yocum, C. F.; Betts, S. D.; Bowlby, N. R. *J. Am. Chem. Soc.* **1990**, 112, 2549–2557. (c) Stemmler, T. L.; Sossong, T. M.; Goldstein, J. I.; Ash, D. E.; Elgren, T. E.; Kurts, D. M., Jr.; Penner-Hahn, J. E. *Biochemistry* **1997**, 36, 9847–9858. (d) Kuzek, D.; Pace, R. J. *Biochim. Biophys. Acta* **2001**, 1503, 123–137. (e) Fernández, G.; Corbella, M.; Alfonso, M.; Stoeckli-Evans, H.; Castro, I. *Inorg. Chem.* **2004**, 43, 6684–6698.
- (36) (a) Phan, N. T. S.; van der Sluys, M.; Jones, C. W. *Adv. Synth. Catal.* **2006**, 348, 609–679. (b) Arends, I. W. C. E.; Sheldon, R. A. *Appl. Catal., A* **2001**, 212, 175–187.